Localized structures in nonlinear optical cavities

Damià Gomila[a,b], Pere Colet[a], Manuel A. Matías[a], Gian-Luca Oppo[b,c] and Maxi San Miguel[a]

[a] Instituto Mediterráneo de Estudios Avanzados (IMEDEA,CSIC-UIB)
Campus Universitat Illes Balears, E-07122 Palma de Mallorca, Spain
[b]University of Strathclyde, 107 Rottenrow, Glasgow G4 0NG, United Kingdom
[c] Centro Studi Dinamiche Complesse, University of Florence, Italy

ABSTRACT

Dissipative localized structures, also known as cavity solitons, arise in the transverse plane of several nonlinear optical devices. We present two general mechanisms for their formation and some scenarios for their instability. In situations of coexistence of a homogeneous and a pattern state, we characterize excitable behavior mediated by localized structures. In this scenario, excitability emerges directly from the spatial dependence since it is absent in the purely temporal dynamics. In situations of coexistence of two homogeneous states, we discuss localized structures either due to the interaction of front tails (dark ring cavity solitons) or due to a balance between curvature effects and modulational instabilities of front solutions (stable droplets).

Keywords: Localized Structures, Cavity solitons, Nonlinear Optical Cavities, Kerr media, Excitability.

1. INTRODUCTION

Localized structures in the transverse plane of nonlinear optical cavities, the so called cavity solitons (CS), have a great potential for application in optical storage and processing of information which have motivated both theoretical and experimental research in the last years.[1–5] CS share a number of fundamental properties with localized structures found in different systems, such as chemical reactions, gas discharges, fluids or granular media.[6–10] In optical cavities these structures appear due to the interplay between diffraction, nonlinearity, external driving, and dissipation. Dissipative solitons have to be distinguished from conservative solitons found for example in propagation in fibers, for which there is a continuous family of solutions depending on their energy. Instead, dissipative solitons are unique once the parameters of the system have been fixed. This uniqueness together with the fact that cavity solitons can be individually written or erased with the help of an additional addressing beam is what makes them useful in optical (i.e., fast and spatially dense) storage and processing of information.[2,5,11,12]

In optical cavities the mechanisms that lead to the formation of stable localized structures can be, very generally, classified in two large groups: i) those that appear in regimes where a homogeneous and a spatially modulated steady states coexist, and ii) those associated with the existence of two homogeneous steady states (also refereed as phases). In the first case, the cavity solitons are solutions connecting the homogeneous steady state with the modulated solution and back to the homogeneous.[13–15] In the second case localized structures are formed by shrinking domains of one phase embedded in the other. The shrinkage is determined by the different stability of both phases and by curvature effects.[16] The walls separating the two phases (domain walls) are typically narrow spatial features whose transverse spatial profile presents damped oscillations due to diffraction. These oscillatory tails may stop the shrinkage leading to the formation of a localized structure which typically appears as a bright spot surrounded by a dark ring and therefore the name of dark ring cavity solitons. They have been described in the optical parametric oscillator where the two homogeneous solutions are equivalent except for a π shift the phase of the electric field[17–20] or in the vectorial Kerr resonator where homogeneous solutions differ in the polarization direction.[21] Within the frame of case ii) where two homogeneous solutions coexist, another kind of stable localized structure has been recently described: the stable droplet.[22,23] It arises as a balance between curvature driven shrinking of a domain and the growth due to the instability of tightly curved fronts. In contrast with dark ring cavity solitons, whose size is typically of the order of a domain wall width

http://www.imedea.uib.es/PhysDept/

and which can exist both in 1-dimensional and 2-dimensional systems, stable droplets are large stable circular domain walls separating the two homogeneous solutions which can only exists in systems whose dimensionality is at least two.[22,23]

Here we analyze two different phenomena of interest for applications of CS to all-optical processing and storage of information. For the sake of simplicity we will consider both phenomena in the same system, a cavity filled with a nonlinear Kerr medium. The appropriate model to describe these cavity is introduced in section 2. In the self-focusing regime, this system displays localized structures of the type i) described above. In section 3 we will consider the instabilities that this kind of structures may develop and in particular we will discuss the existence of an excitable regime. Excitability is a concept arising originally from biology, and it has been found in a variety of systems,[24,25] including optical systems.[26–29] Typically a system is said to be excitable if while it sits at a stable fixed point, perturbations beyond a certain threshold induce a large response before coming back to the rest state. In addition, excitability is also characterized by the existence of a refractory time during which no further excitation is possible. This is the dynamical regime in which cells in the cardiac tissue or neurons in the brain work. Such a regime, associated to CS, provides a potentially useful tool to process optical information in a way similar to assemblies of neurons.

When the polarization of the electric field is taken into account, in the self-defocusing regime the Kerr cavity shows the formation of localized structures of the type ii). In section 4 we will discuss the regimes for which dark ring cavity solitons appear and the regimes where stable droplets are formed.

2. MODEL

We consider an optical cavity filled with a Kerr medium. In the paraxial and mean-field approximations, the evolution of the slowly varying envelopes of the plus and minus circularly polarized components of the electric field $E_\pm$ are described by[30–32]:

$$\partial_t E_\pm = -(1+i\eta\theta)E_\pm + i\nabla^2 E_\pm + E_0 + \frac{1}{4}i\eta[|E_\pm|^2 + \beta|E_\mp|^2]E_\pm \tag{1}$$

where E_0 is the input pump which we will consider as linearly polarized along the x-axis, θ is the cavity detuning, ∇^2 is the transverse Laplacian which models diffraction in the paraxial approximation, β is proportional to the strength of the susceptibility tensor, and $\eta = +1(-1)$ indicates the self-focusing (defocusing) regime. In the scalar case ($E_+ = E_-$), after an appropriate rescaling of the field, Eq. (1) can be reduced to

$$\frac{\partial E}{\partial t} = -(1+i\eta\theta)E + i\nabla^2 E + E_0 + i\eta\,|E|^2\,E. \tag{2}$$

3. EXCITABILITY MEDIATED BY LOCALIZED STRUCTURES

Eq. (2) has an homogeneous solution, given implicitly by $E_s = E_0/(1+i(\theta - I_s))$, where $I_s = |E_s|^2$. The homogeneous solution becomes unstable at $I_s = 1$ leading to the formation of an hexagonal pattern. The bifurcation starts subcritically and the pattern coexists with the homogeneous solution.[30,33] As a result, a stable-unstable pair of CS associated to the periodic solution is formed at a saddle node bifurcation.[14,15] The region of existence of these CS, also known as Kerr cavity solitons, has been characterized in,[13,34] and is partially shown in Fig. 1. Below the solid line there are no CS. At the solid line a pair of CS (one stable and one unstable) are created through a saddle-node bifurcation. In the grey region the soliton is stable. In the honeycomb region the soliton becomes azimuthally unstable leading to an hexagonal pattern. If the dot-dashed line is crossed, either increasing the input intensity or the cavity detuning, the stable CS undergoes a supercritical Hopf bifurcation and starts to oscillate autonomously.[13,34,35] Oscillatory CS exist for parameter values within the region shown with vertical lines in Fig. 1.

The oscillatory regime is shown in detail in fig. 2. Although the amplitude of the soliton oscillates, this regime can still be useful for the purpose of information processing since the amplitude is always significatively larger than background so that the soliton can always be distinguished.[34]

The CS oscillation is such that it approaches the lower-branch CS, which is a saddle point in phase space. As a control parameter is increased, for instance θ, part of the limit cycle moves closer and closer to the lower-branch

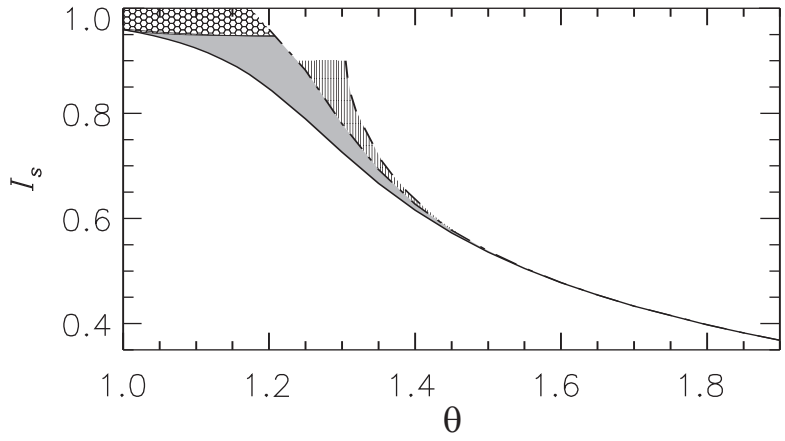

Figure 1. Phase diagram: I_s vs. θ showing the different regimes. CS are stable in the shaded region and oscillate in the dashed one. The solid line indicates the saddle-node bifurcation where the CS are created, the dot-dashed the Hopf, and the dashed the saddle-loop where the oscillation is destroyed.

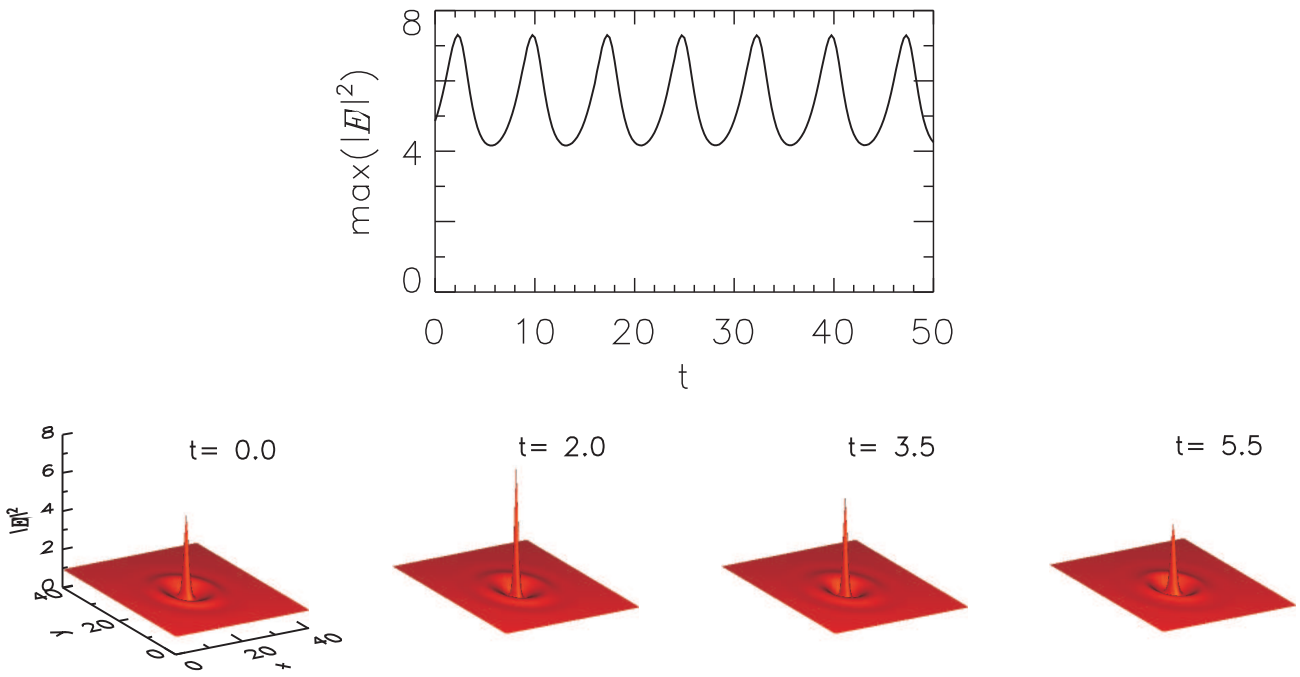

Figure 2. Temporal evolution of the cavity soliton maximum (top) and spatial soliton profile at different times.

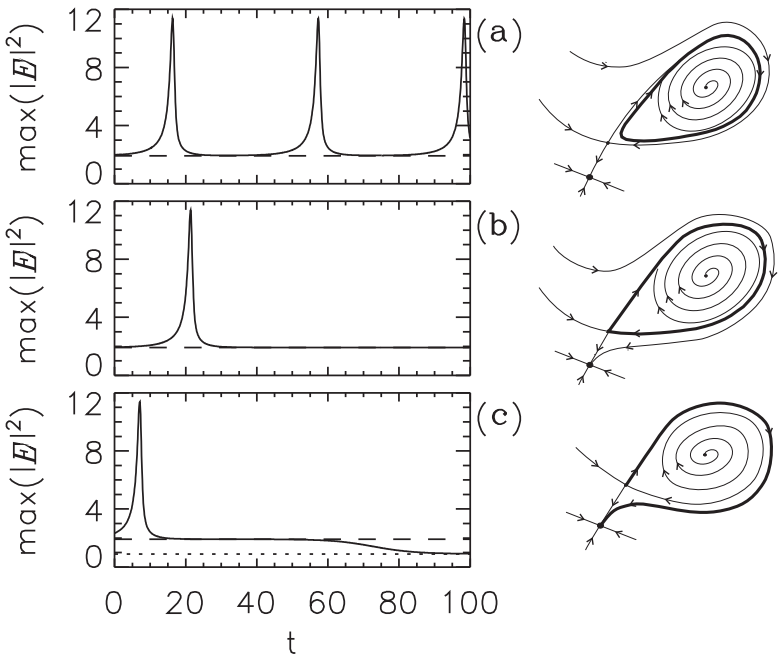

Figure 3. Left: CS maximum intensity as a function of time for increasing values of the detuning parameter θ. From top to bottom $\theta = 1.3047, 1.30478592, 1.304788$. $I_s = 0.9$. Right: Sketch of the phase space for each parameter value. The thick line shows the trajectory of the CS in phase space.

CS, as illustrated in Fig. 3.[36] On the left column we plot the time evolution of the CS maximum obtained from numerical integration of Eq. (2), the dashed line shows for comparison the maximum of the lower-branch CS. On the right column we sketch the evolution on phase space projected on two variables. At a certain critical value a global bifurcation takes place: the cycle touches the lower-branch CS and becomes a homoclinic orbit (Fig. 3b). This is an infinite-period bifurcation called *saddle-loop* or *homoclinic bifurcation*.[37–39] For $\theta > \theta_c$, the saddle connection breaks and the loop is destroyed (Fig. 3c). After following a trajectory in phase space close to the previous loop the CS approaches the saddle point (dashed line) where the evolution is dominated by its slow stable manifold (see the long plateau between $t = 15$ and $t = 60$ in Fig. 3c). Finally the CS decays to the homogeneous solution (dotted line). For larger values of θ the trajectory moves away from the saddle and, therefore, the decay to the homogeneous solutions takes place in shorter times.

The saddle-loop bifurcation has a characteristic *scaling law* that governs the period of the limit cycle as the bifurcation is approached. Close to the critical point the system spends most of the time close to the unstable CS (saddle). The period of the oscillation T can be then estimated by the linearized dynamics around the saddle[37–39]

$$T \propto -\frac{1}{\lambda_1} \ln(\theta_c - \theta), \tag{3}$$

where λ_1 is the unstable eigenvalue of the saddle point. We have verified that this scaling law is verified in our system. Fig. 4 shows the period of the CS limit cycle as a function of the control parameter θ.[36] As expected, the period of the l imit cycle diverges logarithmically as the bifurcation is approached. We then evaluate λ_1 with arbitrary precision from a semi-analytical stability analysis of the unstable CS as in.[34] The lower-branch CS has one single positive eigenvalue $\lambda_1 = 0.177$. In Fig. 4 (right) we plot using crosses the period of the oscillation CS as a function of $ln(\theta_c - \theta)$ obtained from numerical simulations of Eq. (2). Performing a linear fitting we obtain a slope 5.60, in excellent agreement with the theoretical prediction $1/\lambda_1 = 5.65$, proving the existence of a saddle-loop bifurcation for the oscillating CS. We should note that the theory was developed for planar bifurcations, therefore, as the phase space is a plane, the saddle has one unstable direction and one attracting direction.[37–39] The stable manifold of the unstable CS is, however, infinite dimensional. The success of the planar theory to

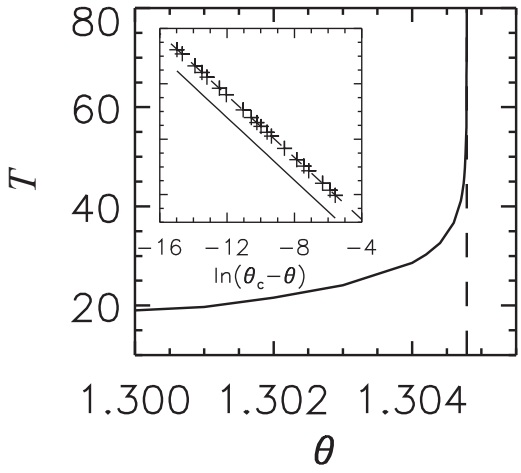

Figure 4. Period of the limit cycle T as a function of the detuning θ for $I_s = 0.9$. The vertical dashed line indicate the threshold of the saddle-loop bifurcation $\theta_c = 1.30478592$. The inset shows T as a function of $\ln(\theta_c - \theta)$. Crosses correspond to numerical simulations while the solid line has a slope $1/\lambda_1$ with $\lambda_1 = 0.177$ obtained from the linear stability analysis of the lower-branch CS.

describe our infinite dimensional system can be attributed to the fact that, somehow, the dynamics of the CS is effectively two-dimensional with a single unstable manifold and an effective stable manifold.

In systems without spatial dependence it has been shown that an scenario composed by a saddle-loop bifurcation and a stable fixed point leads to a excitability regime (class-I excitability in which the response time is unbounded).[29, 40, 41] In our infinite-dimensional system CS does indeed show en excitable behavior: the homogeneous solution is a globally attracting fixed point but localized disturbances (above the lower-branch CS) can send the system on a long excursion through phase space before returning to the fixed point.[36]

Fig. 5 shows the resulting trajectories of applying a perturbation in the direction of the unstable CS with three different intensities: one below the excitability threshold (dotted line), and two above: one very close to threshold (dashed line) and the other well above (solid line). In the first case the system relax exponentially to the homogeneous solution, while in the latter two cases it perform a long excursion before returning to the stable fixed point. In the case of a near threshold excitation the refractory period is appreciably longer due to the effect of the saddle. The spatial profile of the localized structure is shown in Fig. 6. The peak grows to a large value until the losses stop it. Then it decays exponentially until it disappears. A remnant wave is emitted out of the center dissipating the remaining energy.

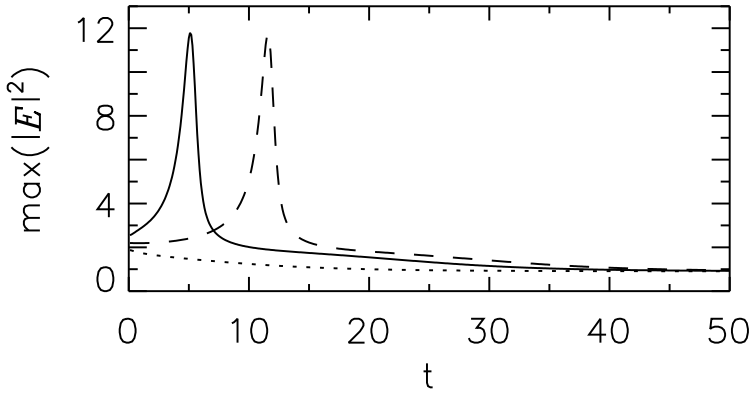

Figure 5. Time evolution of the soliton maximum starting from the homogeneous solution ($I_s = 0.9$) plus a localized perturbation of the form of the unstable CS multiplied by a factor 0.8 (dotted line); 1.01 (dashed line) and 1.2 (solid line).

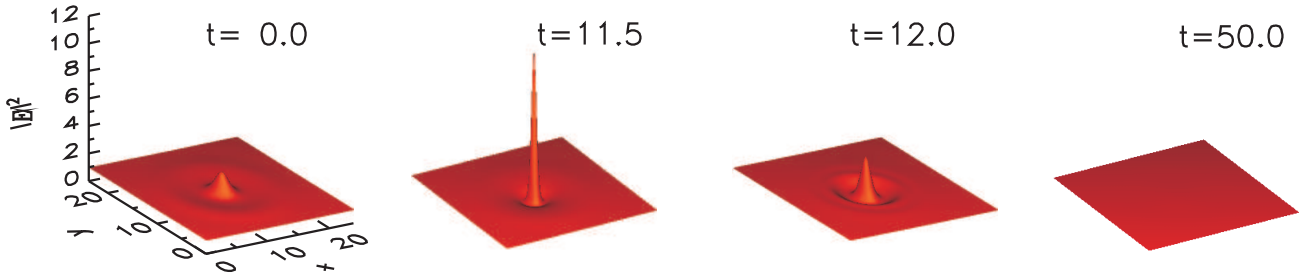

Figure 6. Soliton profile at different times for the trajectory shown as dashed line in Fig. 5

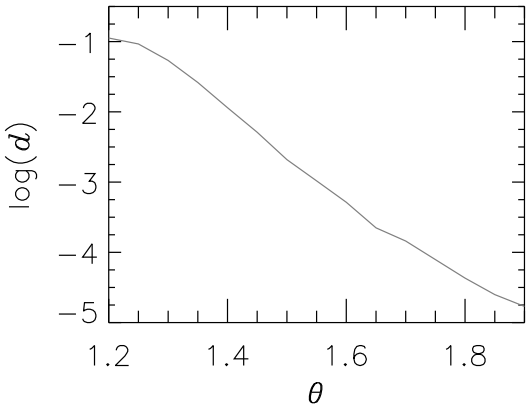

Figure 7. Distance between the saddle-node and the Hopf lines.

There is an important point to notice. Without spatial dependence Eq. (2) does not show any excitable behavior while the localized structures that appear in the spatially dependent system do. Thus excitability appears as an emergent property mediated by localized structures.[36]

In the limit of large detuning, the saddle-node, Hopf and saddle-loop bifurcation lines meet asymptotically at $I_s = 0$ as shown in Fig. 7, with the frequency of the Hopf bifurcation going to zero.[36] It is known that such intersection of a saddle-node line with a Hopf line is a Takens-Bogdanov (TB) codimension-2 bifurcation point.[42,43] The unfolding around a TB point leads to a saddle-loop bifurcation line.[42,43] So, this unfolding fully explains the observed scenario, where once again our formally infinite-dimensional system appears to be perfectly described by a dynamical system in the plane.

The TB point occurs asymptotically in the limit of large detuning θ and small pump E_0. This limit corresponds to the case in which Eq. (2) becomes the conservative non linear Schrodinger eq..[35,44] Excitable behavior is, then, an intrinsic property of 2D solitons in this equation and therefore has implications in a wide variety of physical systems, in particular in nonlinear optics.

4. STABLE POLARIZATION DROPLETS AND CAVITY SOLITONS

We consider the case of a vectorial Kerr cavity described by Eq. (1). For $E_0 < E_{th} \approx 0.95$, Eq. (1) has a stable homogeneous symmetric solution $I_+ = I_-$ (where $I_\pm = |E_\pm|^2$).[32] In what follows we will consider $\theta = 1$ and $\beta = 7$. Above this threshold, a y-polarized stripe pattern is formed. For pump values above a second threshold, $E_0 \approx 1.5$, the system has two bistable homogeneous solutions, namely $E_\pm^a$ and $E_\pm^b$, which are asymmetric ($I_+^{a,b} \neq I_-^{a,b}$) and therefore elliptically polarized. These two solutions are equivalent in the sense that $E_\pm^a = E_\mp^b$, so that they have the same total intensity, polarization ellipticity and stability properties for all values of the control parameter. They differ in the orientation and in the direction of rotation of the polarization ellipse. A domain of one of these homogeneous solutions embedded in the other can therefore be identified as a polarization

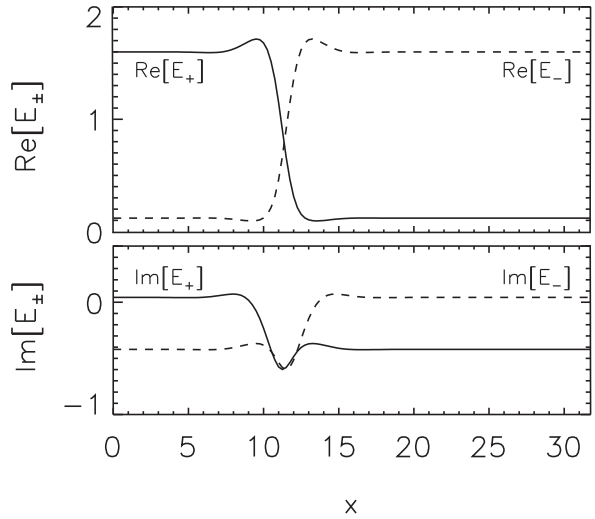

Figure 8. Profile of the $d = 1$ front connecting the two equivalent homogeneous solutions of the VKR for $E_0 = 1.6$.

domain. A $d = 1$ front connecting these two solutions is narrow spatial feature presenting damped oscillations in the tails due to diffraction (see Fig. 8). The shape of these fronts has been obtained by solving numerically the $d = 1$ stationary form of Eq. (1) and imposing zero derivative as boundary conditions.

For one transverse dimension $d = 1$, a front connecting the two states does not move since they are equivalent. However for $d = 2$ these fronts may move due to curvature effects.[22] For simplicity let us consider the movement of a domain with circular symmetry where the curvature κ is the inverse of the radius R. It turns out that the radius of a circular domain of one solution embedded in the other evolves in time as

$$\dot{R}(t) = -\gamma(E_0)/R \tag{4}$$

where E_0 is a the control parameter. From the $d = 1$ front profile and following the procedure indicated in 22 we determine the value of the growth coefficient for a circular domain γ. Since the front profile depends on the pump strength E_0, the value of γ will also be dependent on E_0 as shown in Fig. 9.

The coefficient γ may changes sign upon variations of the control parameter.[21–23] We identify the value

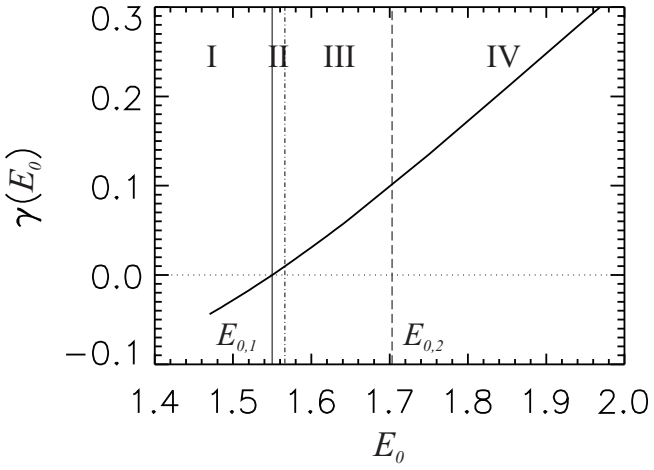

Figure 9. Growth rate γ versus the pump E_0 for the vectorial Kerr resonator. The vertical solid line indicates the modulational instability threshold for the flat front $E_{0,1} = 1.550$ and the vertical dashed line indicates the upper limit of existence of localized structures $E_{0,2} = 1.703$. Stable droplets exist in region II and dark ring cavity solitons in region III

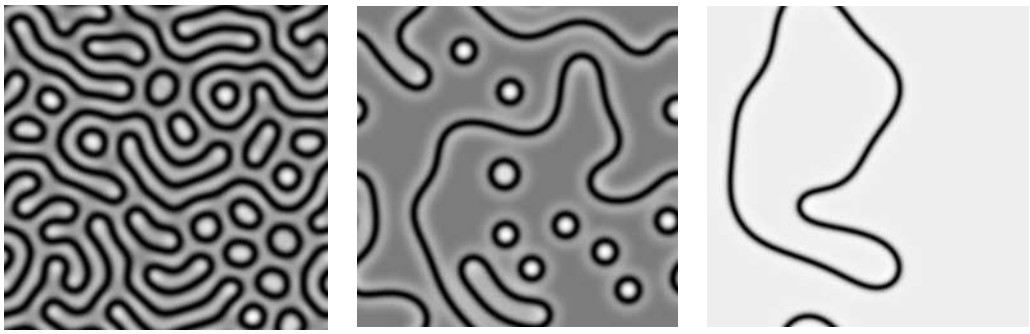

Figure 10. From left to right, snapshots of typical configurations of the total intensity $I_+ + I_-$ in the labyrinthine, localized structures and coarsening regimes.

$E_0 = E_{0,1}$ of the control parameter for which γ vanishes, and $\gamma > 0$ ($\gamma < 0$) for $E_0 > E_{0,1}$ ($E_0 < E_{0,1}$). When γ is positive and large, any circular polarization domain with large radius shrinks. It is observed that arbitrarily shaped domains also shrink and the typical domain size decreases as in Eq.(4). If γ is negative, any circular domain will grow due to curvature effects. In addition, any perturbation of a wall grows so that in this regime a flat wall is modulationally unstable and a generic initial condition evolves into labyrinthine patterns. Thus $E_{0,1}$ signals the place at which a flat wall connecting the two equivalent states becomes modulationally unstable. Therefore, depending on the value of γ, three dynamical regimes can be identified when increasing the control parameter E_0 (see Fig. 10)[21,23]: a regime of labyrinthine pattern formation for $E_0 < E_{0,1}$ (region I), a regime of formation of localized structures for $E_{0,1} < E_0 < E_{0,2}$ (regions II and III) and a regime of domain coarsening for $E_0 > E_{0,2}$ (region IV). These three regimes have been experimentally observed in a four wave mixing resonator.[45]

We now discuss the different CS that appear in this system. Figure 11 shows the radius and the typical profile of the CS as function of the pump strength. It has been calculated by numerically solving the stationary radial equation with zero derivative at the origin and at the external boundary.[20] The solid (dotted) line corresponds to the radius of stable (unstable) localized structures. Two kinds of stable CS can be clearly distinguished, the dark ring cavity solitons and the stable droplets. The unstable localized structures which have a shape similar to that of the stable dark ring cavity solitons but with smaller amplitude.

Dark ring cavity solitons appear in region III since the shrinking of a domain is halted by the interaction of the front oscillatory tails. This interaction, which is stronger for larger oscillation amplitudes, is precisely what provides stability to these structures. For a certain class of $d = 1$ systems, and under some approximations, it has been shown that the interaction of two distant fronts can be described by a potential with several wells which become progressively deeper the shorter the distances between the fronts.[46] The wells of the interaction potential are located at the distances where the extrema of the oscillations of the tails aver lap with each other. Typically nonlinear optical cavities such as the one considered here does not belong to this class of systems, but equilibrium distances are also found whenever the extrema of the local oscillations of the domain wall overlap with each other.[20] For the vectorial Kerr cavity we found that only the locking at the first maxima of the oscillations is effective to counterbalance the shrinking. In this respect we should notice an important difference between the $d = 1$ and $d = 2$ cases. In $d = 2$, increasing the pump there is a threshold ($E_0 = E_{0,2}$, see Figs. 9, 11) for the interaction of the local oscillations to counterbalance the shrinking of the circular domains due to the local curvature of the walls. It may appear counterintuitive that dark ring cavity solitons lose their stability for increasing pump intensities where one would expect diffraction to be more effective. The amplitude of the local oscillations at the tails of the fronts however, has a complex dependence on the parameters of the system and decreases for increasing input energies. Furthermore, it is clear from Fig. 9 that the coefficient γ grows with the pump; therefore the shrinking force due to front curvature becomes more important, overcoming the interaction of the tails at $E_0 = E_{0,2}$. In terms of stationary solutions, this threshold corresponds to a saddle-node bifurcation where the stable and the unstable branches of the dark ring cavity solitons collide (Fig. 11). No CS are observed for pump values larger than $E_{0,2}$, indicating that this is the threshold for domain coarsening.

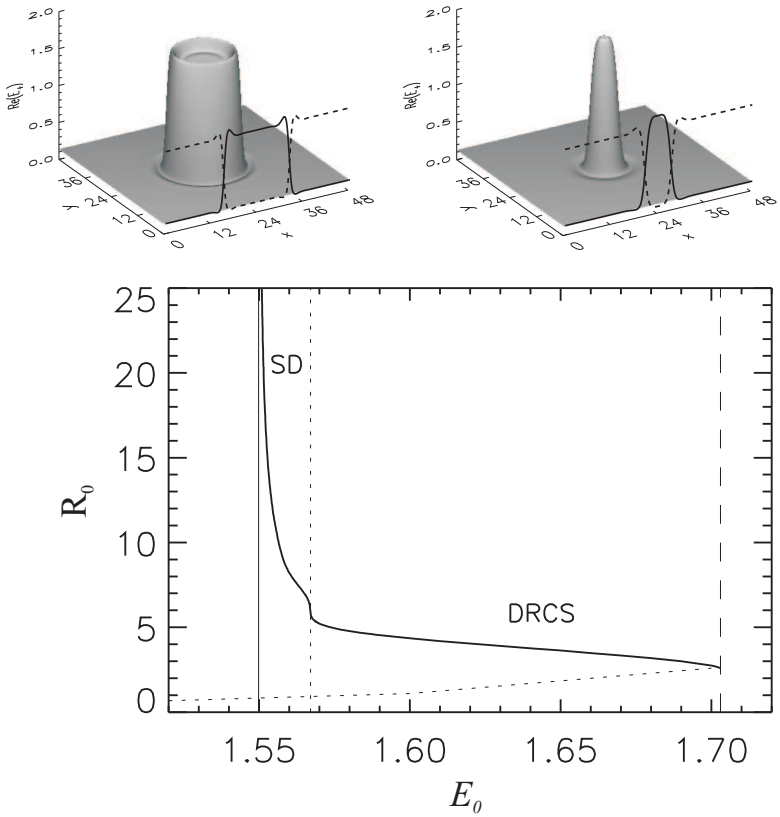

Figure 11. Radius of the cavity solitons as a function of the pump parameter E_0. Solid (dotted) lines correspond to stable (unstable) CS. The vertical solid line indicates $E_{0,1}$, the vertical dashed line indicates $E_{0,2}$ and the vertical dotted line indicates $E_{0,3}$, the transition from dark ring cavity solitons to stable droplets. The figures on the top show the profile of a stable droplet ($E_0 = 1.55238$) (left) and a dark ring cavity soliton (right) ($E_0 = 1.6$). The solid (dashed) line corresponds to the real part of E_+ (E_-) along a central section.

We focus now on the region close to the modulational instability of the flat domain wall but for $E_0 > E_{0,1}$. Close to the point $E_{0,1}$ where γ vanishes, higher order corrections to Eq. (4) must be considered.[22,23] An amplitude equation for the curvature κ of gently curved fronts can be derived for a rather general class of systems which include the nonlinear optical cavities considered here.[22] One obtains that the dynamics of a circular domain of radius R, is given by the equation[22]

$$\dot{R} = -c_1(E_0 - E_{0,1})\frac{1}{R} - c_3\frac{1}{R^3}, \tag{5}$$

where the coefficients c_1 and c_3 can be calculated from the profile of the $d = 1$ front connecting the two equivalent solutions at $E_0 = E_{0,1}$ following the procedure indicated in Ref. 22. For the nonlinear Kerr cavity model considered here, $c_1 = 0.591$ and $c_3 = -0.393$, therefore Eq. 5 predicts just above $E_{0,1}$ the existence of stable stationary circular domains (the stable droplet) with a radius R_0 given by

$$R_0 = \frac{1}{\sqrt{E_0 - E_{0,1}}}\sqrt{\frac{-c_3}{c_1}}. \tag{6}$$

For E_0 larger than but close to $E_{0,1}$ an initially small (very large) domain grows (shrinks) until a stable droplet is formed. Note that the radius of the stable droplet diverges at $E_{0,1}$. Furthermore it can be shown on rather general grounds[22] that domains of arbitrary shape evolve first to circular domains and then to stable droplet, making the stable droplet an attractor and the most relevant localized structure for values of the control parameter just above the modulational instability of the flat domain wall.

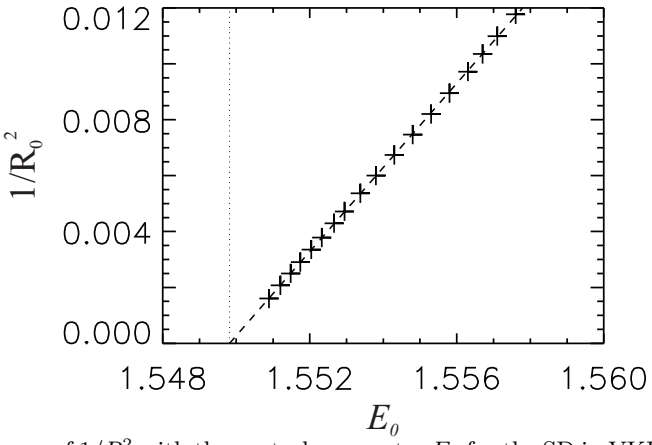

Figure 12. The linear dependence of $1/R_0^2$ with the control parameter E_0 for the SD in VKR. The dotted line corresponds to Eq. (6) with $c_1 = 0.591$ and $c_3 = -0.393$, while the crosses are from the numerical determination of the SD as steady states of Eq. (1).

Figure 11 shows the radius and the profile of the stable droplets found in our system obtained solving the stationary radial equation. The stable droplet is in fact an elliptically polarized domain embedded in a background with opposite elliptical polarization and therefore it constitutes a cavity polarization soliton. At the center of the stable droplet, the field takes the value of one of the homogeneous solutions. Depending on the value of the pump, the radius of the stable droplet can be extremely large. In fact, the radius diverges at $E_{0,1}$ as $R_0 \approx 1/\sqrt{E_0 - E_{0,1}}$. Figure 12 shows a comparison of $1/R_0^2$ between the theoretical prediction given by Eq. (6) (dotted line in Figure 12) and numerical results (crosses) in the vicinity of $E_{0,1}$ (vertical solid line). The agreement is excellent thus demonstrating that stable droplets are a universal feature of systems with modulational instability of the flat front.

Moving now in the direction of increasing E_0, we find that the stable droplet branch has a change of behavior at $E_0 = E_{0,3}$ (see Fig. 11). This particular point corresponds to the value of the pump for which the interaction of the tails becomes of the same order as the nonlinear correction of Eq. (5). We note that the transition from dark ring cavity solitons to stable droplets is continuous and that the last nucleates out of the former. Such a transition is, however, marked by a sudden change in the size of the CS. While the radius of the dark ring cavity soliton changes very little with decreasing control parameter E_0, the radius of the stable droplet changes rapidly with $(E_0 - E_{0,1})$ as shown in Eq. (6). For $E_{0,3} < E_0 < E_{0,2}$ the interaction of the oscillatory tails is dominant and the CS is a dark ring cavity soliton. For $E_{0,1} < E_0 < E_{0,3}$ the nonlinear curvature effects (including the growth which leads to the SD) dominate over the interaction of the oscillatory tails and a stable stationary circular domain wall is formed.

5. CONCLUSIONS

We have identified two general mechanisms for the formation of localized structures (cavity solitons) in models of nonlinear optical devices. In the first one, coexistence between a homogeneous and a pattern state leads to the formation of peaked cavity solitons of size comparable to the pattern spatial wavelength. By changing appropriate control parameters, these CS solutions first become unstable to periodic oscillations and then approach a homoclinic bifurcation that lead to their disappearance. Once the homogeneous solution remains the only stable solution, the presence of the unstable CS solution leads to a novel regime of excitability that is localized in space and has no counterpart in the purely temporal dynamics of the systems where spatial effects have been removed.

The second general mechanism of formation of CS requires the simultaneous presence of two homogeneous solutions. In these systems, solitary walls connecting the two homogeneous solutions are commonplace. A peculiar feature of diffraction is to introduce local oscillations in the vicinity of the wall solutions. In two transverse dimensions, these local oscillations interact and lock spatially localized solutions known as dark ring solitons because of what remains of the original circular wall. Under appropriate changes of the control

parameters, we have approached the modulational instability of a flat domain wall. Before reaching the critical parameter values, stable droplets can be found. These are circular domains whose radius is unstable to curvature effects if too large and to the incipient modulational instability of the flat front if too small. It is interesting to note that in systems such as optical parametric oscillators dark ring cavity solitons can nest inside a stable droplet (see Ref. 23).

Finally we note that for excitability, stable droplets and dark ring cavity solitons we have derived analytical and exact scaling laws. It is our belief that excursion from these predicted values (see several references in 47) maybe artefacts due to finite size of the numerical simulations.

ACKNOWLEDGMENTS

We acknowledge financial support from the European Commission project QUANTIM (IST-2000-26019). P. Colet, M.A. Matias and M. San Miguel acknowledge financial support from MEC (Spain) and FEDER: Grant Nos. BFM2001-0341-C02-02, FIS2004-00953, and FIS2004-05073-C04-03. D. Gomila acknowledges financial support from EPSRC (Grant No. GR/S28600/01). G.-L. Oppo acknowledges support form SGI, the Royal Society Leverhulme Trust, the PCRI consortium of the University of Strathclyde and EPSRC (Grant No. GR/R04096) and EU project FunFACS.

REFERENCES

1. Feature section on cavity solitons, L.A. Lugiato ed., *IEEE J. Quant. Elect.* **39**, No. 2 , 2003;
2. Special issue on solitons, *Opt. Photon. News* **13**, pp. 27-76, 2002.
3. M. Tlidi, P. Mandel, and R. Lefever, "Localized structures and localized patterns in optical bistability", *Phys. Rev. Lett.* **73**, pp. 640-643, 1994.
4. B. Schäpers, M. Feldmann, T. Ackemann, and W. Lange, "Interaction of localized structures in an optical pattern-forming system", *Phys. Rev. Lett.* **85**, pp. 748-751, 2000.
5. S. Barland, J.R. Tredicce, M. Brambilla, L.A. Lugiato, S. Balle, M. Giudici, T. Maggipinto, L. Spinelli, G. Tissoni, T. Knödl, M. Miller and R. Jäger, "Cavity solitons as pixels in semiconductor microcavities" *Nature* **419**, pp. 699-702, 2002.
6. O. Thual and S. Fauve, "Localized structures generated by subcritical instabilities" *J. Phys.* **49**, pp. 1829-1833, 1988.
7. J.E. Pearson, "Complex patterns in a simple system", *Science* **261**, pp. 189-192, 1993.
8. K.J. Lee, W.D. McCormick, Q. Ouyang, and H.L. Swinn, "Pattern formation by interacting chemical fronts", *Science* **261**, pp. 192-194, 1993.
9. I. Müller, E. Ammelt, and H.G. Purwins, "Self-organized quasiparticles: breathing filaments in a gas discharge system" *Phys. Rev. Lett.* **82**, pp. 3428-3431, 1999.
10. P. Umbanhowar, F. Melo, and H.L. Swinney, "Localized excitations in a vertically vibrated granular layer", *Nature* **382**, pp. 793-796, 1996.
11. W.J. Firth and A.J. Scroggie,"Optical bullet holes: robust controllable localized states of a nonlinear cavity", *Phys. Rev. Lett.*, **76**, pp. 1623-1626, 1996.
12. W.J. Firth and G.K. Harkness, "Cavity solitons", *Asian Journal of Physics*, **7**, pp. 665-677, 1998.
13. W.J. Firth, A. Lord, and A.J. Scroggie, "Optical bullet holes", *Physica Scripta* **67**, pp. 12-16, 1996.
14. P. Coullet, C. Riera, and C. Tresser, "Stable static localized structures in one dimension", *Phys. Rev. Lett.* **84**, pp. 3069-3072, 2000
15. P. Coullet, C. Riera, and C. Tresser, "A new approach to data storage using localized structures", *Chaos* **14**, pp. 193-198, 2004.
16. D. Gomila, P. Colet, G.-L. Oppo and M. San Miguel, "Stable droplets and nucleation in asymmetric bistable nonlinear optical systems", *J. Opt. B: Quantum Semiclass. Opt.*, **6**, pp. S265-S270, 2004.
17. K. Ouchi and H. Fujisaka, "Phase ordering kinetics in the Swift-Hohenberg equation", *Phys. Rev. E*, **54**, pp. 3895-3898, 1996.
18. K. Staliunas and V.J. Sanchez-Morcillo, "Spatial-localized structures in degenerate optical parametric oscillators", *Phys. Rev. A*, **57**, pp. 1454-1457, 1998.

19. G.-L. Oppo, A.J. Scroggie and W.J. Firth, "From domain walls to localized structures in degenerate optical parametric oscillators", *J. Opt. B: Quantum Semiclass. Opt.*, **1**, pp. 133-138, 1999.
20. G.-L. Oppo, A.J. Scroggie and W.J. Firth, "Characterization, dynamics and stabilization of diffractive domain walls and dark ring cavity solitons in parametric oscillators", *Phys. Rev. E*, **63**, pp. 066209-1-16, 2001.
21. R. Gallego, M. San Miguel and R. Toral, "Self-similar domain growth, localized structures, and labyrinthine patterns in vectorial Kerr resonators", *Phys. Rev. E*, **61**, pp. 2241-2244, 2000.
22. D. Gomila, P. Colet, G.-L. Oppo and M. San Miguel,"Stable Droplets and Growth Laws Close to the Modulational Instability of a Domain Wall", *Phys. Rev. Lett.*, **87**, pp. 194101-1-4, 2001.
23. D. Gomila, P. Colet, M. San Miguel, A.J. Scroggie, and G.-L. Oppo, "Stable droplets and dark-ring cavity solitons in nonlinear optical devices", *IEEE J. Quantum Electron.*, **39**, pp. 238-244, 2003.
24. E. Meron, "Pattern formation in excitable media", *Phys. Rep.* **218**, pp. 1-66, 1992.
25. J.D. Murray, *Mathematical Biology*, 3rd Ed., Springer, 2002.
26. H.J. Wünsche, O. Brox, M. Radziunas, and F. Henneberger, "Excitability of a semiconductor laser by a two-mode homoclinic bifurcation", *Phys. Rev. Lett.* **88**, pp. 023901-1-4, 2002.
27. S. Barland, O. Piro, M. Giudici, J.R. Tredicce, and S. Balle, "Experimental evidence of van der Pol-Fitzhugh-Nagumo dynamics in semiconductor optical amplifiers", *Phys. Rev. E* **68**, pp. 036209-1-6, 2003.
28. J.L.A. Dubbeldam, B. Krauskopf, and D. Lenstra, "Excitability and coherence resonance in lasers with saturable absorber", *Phys. Rev. E* **60**, pp. 6580-6588, 1999.
29. F. Plaza, M.G. Velarde, F.T. Arecchi, S. Boccaletti, M. Ciofini and R. Meucci, "Excitability following an avalanche-collapse process", *Europhys. Lett.* **38**, pp. 85-90, 1997.
30. L.A. Lugiato and R. Lefever, "Spatial dissipative structures in passive optical systems", *Phys. Rev. Lett.* **58**, pp. 2209-2211, 1987.
31. J.B. Geddes, J.V. Moloney, E.M. Wright and W.J. Firth, "Polarisation patterns in a nonlinear cavity", *Opt. Comm.*, **111**, pp. 623-631, 1994.
32. M. Hoyuelos, P. Colet, M. San Miguel, and D. Walgraef, "Polarization patterns in Kerr media", *Phys. Rev. E*, **58**, pp. 2292-3007, 1998.
33. A.J. Scroggie, W.J. Firth, G.S. McDonald, M. Tlidi, R. Lefever and L.A. Lugiato, "Pattern formation in a passive Kerr cavity " *Chaos, Solitons, and Fractals* **4**, pp. 1323-1354, 1994.
34. W.J. Firth, G.K. Harkness, A. Lord, J.M. McSloy, D. Gomila and P. Colet, "Dynamical properties of two-dimensional Kerr cavity solitons" *J. Opt. Soc. Am. B* **19**, pp. 747-752, 2002.
35. D.V. Skryabin, "Energy of the soliton internal modes and broken symmetries in nonlinear optics", *J. Opt. Soc. Am. B* **19**, 529-536, 2002.
36. D. Gomila, M.A. Matias and P. Colet, "Excitability mediated by localized structures in a dissipative nonlinear optical cavity", *Phys. Rev. Lett.*, **94**, pp. 063905-1-4, 2005.
37. P. Gaspard, "Measurement of the instability rated of a far-from-equilibrium steady state at an infinite period bifurcation" *J. Phys. Chem.* **94**, pp. 1-3, 1990.
38. P. Glendinning, *Stability, instability, and chaos*, Cambridge U.P., Cambridge, UK, 1994.
39. S. Strogatz, *Nonlinear Dynamics and Chaos*, Addison Wesley, Reading, MA, 1994.
40. J. Rinzel and G.B. Ermentrout, "Analysis of neural excitability and oscillations" in *Methods in Neuronal Modeling*, edited by C. Koch and I. Segev, MIT Press, Cambridge, MA, 1989.
41. E.M. Izhikevich, "Neural excitability, spiking and bursting", *Int. J. Bif. Chaos* **10**, pp. 1171-1266, 2000.
42. J. Guckenheimer and P. Holmes, *Nonlinear Oscillations, Dynamical Systems, and Bifurcations of Vector Fields*, Springer, New York, 1983.
43. Y. A. Kuznetsov, *Elements of Applied Bifurcation Theory, 2nd ed.*, Springer Verlag, New York, 1998.
44. W.J. Firth and A. Lord, "Two-dimensional solitons in a Kerr cavity", *J. Mod. Opt.* **43**, pp. 1071-1078, 1996.
45. V.B. Taranenko, K. Staliunas, and C.O. Weiss, "Pattern formation and localized structures in degenerate optical parametric mixing", *Phys. Rev. Lett.*, **81**, pp. 2236-2239, 1998
46. P. Coullet, C. Elphick and D. Repaux, "Nature of spatial chaos", *Phys. Rev. Lett.*, **65**, pp. 431-434, 1987.
47. P. Mandel and M. Tlidi, "Transverse dynamics in cavity nonlinear optics (2000-2003)", *J. Opt. B* **6**, pp. R60-R75, 2004.